Computational study of aero-optical distortions by a turbulent wake

By A. Mani, M. Wang† AND P. Moin

1. Motivation and objectives

Optical aberrations induced by turbulent flows are a serious concern in airborne communication and imaging systems. In these applications an optical beam is required to be transmitted through a relatively long distance, over which the quality of the beam can degrade due to variations of the index of refraction along its path. For air and many fluids, the refractive index is linearly related to the density of the fluid through the Gladstone-Dale relation (see Wolf & Zizzis 1978), and therefore density fluctuations due to flow turbulence are the root cause of optical aberrations. An airborne optical beam generally encounters two distinct turbulent flow regimes: the turbulence in the vicinity of the aperture produced by the presence of solid boundaries, and atmospheric turbulence.

Aero-optics is the study of optical distortions by the near-field turbulent flows, typically involving turbulent boundary layers, mixing layers, and wakes (see Gilbert 1982). The depth of the aberrating flowfield is usually smaller than or comparable to the projecting (or imaging) aperture. When an initially planar optical wavefront passes a compressible flow, different parts of the wavefront experience different density in the medium and hence have different propagation speeds. Consequently the wavefront becomes deformed. A small initial deformation of the wavefront can lead to large errors on a distant target. The consequences of such deformations include optical beam deflection (bore-sight error) and jitter, beam spread, and loss of intensity. Wavefront distortions can also cause reductions of resolution, contrast, effective range, and sensitivity for airborne electro-optical sensors and imaging systems (Jones & Bender 2001).

Research in the area of turbulent distortions of optical waves can be traced back to the 1950s and 1960s (see, for example, Chernov 1960; Tatarski 1961) when the scattering of acoustic and electromagnetic waves due to random fluctuations of refractive index were studied, mostly in the context of atmosphere propagation. Most of the early studies are based on statistical analysis with simplifying assumptions such as homogeneous and isotropic turbulence, and therefore are not directly applicable in realistic aero-optical flowfields. Sutton (1969) characterized different regimes based on optical and flow parameters for the case of homogeneous and isotropic turbulence and developed statistical models to predict far-field optical aberrations.

It was in the late 1980s when aero-optics in the modern sense, i.e., the study of optical distortions due to near-aperture turbulence, came into consideration. Many experimental studies have been performed to develop high-speed wavefront measurement tools (e.g., Jumper & Fitzgerald 2001; Cheung & Jumper 2004), study the refractive index structures (e.g., Catrakis & Aguirre 2004; Dimotakis *et al.* 2001; Fitzgerald & Jumper 2004), develop distortion scaling laws (e.g., Gordeyev *et al.* 2003), and devise control techniques to suppress or modify optically important turbulence structures (e.g., Gordeyev *et al.* 2004; Sinha *et al.* 2004). Despite advances in wavefront sensor technology, significant limitations

† Present address: Department of Aerospace and Mechanical Engineering, University of Notre Dame

still exist in terms of spatial and temporal resolutions. Computational studies, when performed adequately, can allow us to probe the flow and optical fields in greater detail and hence complement experiments to further our understanding in this area.

Earlier computational approaches for aero-optics typically involved Reynolds-Averaged Navier-Stokes (RANS) calculations using a turbulence model such as the k-ε model, from which crude algebraic relationships were used to obtain the root-mean-square (rms) of intensity and length scales of the index of refraction field. Smith & Truman (1990) used a more sophisticated approach, in which a model transport equation for the rms refractive index fluctuations was solved. The turbulence information was then fed into an optics model based on geometric optics, which predicts properties of the beam such as amplitude loss and spreading. Truman (1992) and Truman & Lee (1990) were among the first to perform time-accurate computational studies of aero-optical distortions. They used direct numerical simulation (DNS) of a homogeneous shear flow and turbulent channel flow to study the induced optical wavefront errors. The simulations were based on incompressible flow equations at relatively low Reynolds numbers, and the fluctuating refractive index was modeled by a passive scalar. The anisotropy of the optical phase errors due to anisotropy of the flow was noted in their work.

Because of its ability to resolve large-scale motions at a reasonable computational cost, Large-Eddy Simulation (LES) has recently been used for aero-optics. Childs (1993) carried out LES of a compressible turbulent mixing layer and performed ray tracing through it. Jones & Bender (2001) used LES to study aero-optical distortions in a fuselage/turret configuration. They used ray tracing to obtain the wavefront error and represented it in terms of Zernike polynomials. Also, they studied instantaneous far-field intensity patterns using the Fraunhofer approximation. Tromeur *et al.* (2003) used LES to study aero-optics of a supersonic boundary layer. Sinha *et al.* (2004) used experiments and LES to investigate control of flowfields to mitigate the distortion of a laser beam passing through a cavity shear layer. In these works the major contribution to optical distortions was assumed to be from the large resolved scales of the flow. The grid resolutions were poor in the cases involving complex geometries, and the numerical schemes employed were either total variation diminishing (TVD) or upwinding techniques that are highly dissipative. This can severely impact the effectiveness of the subgrid scale (SGS) model and artificially damp the small resolved scales of the flow (see Mittal & Moin 1997), which can be important.

The present study is concerned with the numerical simulation of a compressible turbulent wake and its aero-optical effects. We consider the propagation of an optical beam through the flow over a circular cylinder at Reynolds number of 3900 and freestream Mach number of 0.4. The time-dependent refractive-index (density) field is computed using LES, and the time series of distorted optical wavefronts and far-field intensity are obtained using a combination of ray tracing and Fourier optics. An important distinction between the present study and the previous studies is that the numerical scheme is based on a non-dissipative staggered-mesh formulation, which leads to more accurate representations of a wide range of optically important flow scales.

2. Accomplishments

2.1. *Flow simulation*

The compressible flow over a circular cylinder at $Re_D = 3900$ and $M = 0.4$ is computed by LES, using a sixth-order, energy conservative, compact finite difference scheme de-

	C_d	$-C_{p_b}$	St	θ_{sep}	U_{min}
Experiments†	0.99 ± 0.05	0.88 ± 0.05	0.215 ± 0.005	86 ± 2.5	-0.24 ± 0.1
LES‡	1.00	0.95	0.203	85.8	-0.32
LES¶	1.00	0.93	0.207	86.9	-0.35
LES‖	1.04	0.94	0.210	88.0	-0.37
LES††	0.97	0.85	0.213	88.2	-0.31
Present, $M = 0.2$	0.99	0.86	0.206	86.3	-0.33
Present, $M = 0.4$	1.18	1.08	0.202	87.1	-0.26

TABLE 1. Comparison of global flow statistics for flow over a circular cylinder at $Re = 3900$. The parameters from left to right are drag coefficient, base pressure coefficient, Strohal number, separation angle, and minimum averaged streamwise velocity.

† see Kravchenko & Moin (1998)
‡ Beaudan & Moin (1994)
¶ Mittal & Moin (1997)
‖ Kravchenko & Moin (1998)
†† Rizzetta *et al.* (2003)

veloped by Nagarajan *et al.* (2003). The LES code, originally written for a C-mesh, has been modified for a generalized O-mesh to enhance grid smoothness and hence numerical stability. The numerical scheme uses implicit time advancement near the wall and third-order Runge-Kutta away from the wall. The dynamic SGS model for compressible flow by Moin *et al.* (1991) with modification of Lilly (1992) is used to account for the effect of the SGS on the flow.

The computational domain has a radius of approximately $20D$ (D = cylinder diameter) and a width of πD in the spanwise direction. The discretization of the code is based on a generalized curvilinear coordinate formulation. The mesh size is $288 \times 200 \times 48$ in the wall normal, azimuthal, and spanwise directions, respectively. A sponge layer is applied at the outer boundary to make it non-reflecting. The total integration time was over 70 shedding cycles. From the last 14 shedding cycles of the simulation, approximately 800 snapshots of the density field were saved for aero-optical study.

The literature includes several numerical and experimental investigations of incompressible flow over a cylinder at Reynolds number of 3900, which are used to help validate our results. Because all those studies are in the incompressible regime, we performed a Mach 0.2 simulation for validation and a Mach 0.4 simulation for aero-optical study. The validation is appropriate, because at Mach 0.2 the compressibility effect on flow statistics is expected to be relatively small.

Table 2.1 compares the major statistics of our simulations with the previously published ones. For the case of Mach 0.2 the global statistics are consistent with other studies. At Mach 0.4 there is a small difference in the drag coefficient, which is attributed to the effect of compressibility. Figure 1 shows the energy spectra of the vertical velocity in the wake centerline five diameters behind the cylinder. As shown in the figure, the present simulation successfully captures the details of the experimental spectrum, including very high frequency components. The two spectral peaks (at the vortex shedding frequency and its third harmonic) are captured very accurately. Contours of the instantaneous vorticity magnitude in a spanwise cut at a given time are shown in Fig. 2. The two separated shear layers and the development of the Karman vortex street are clearly seen and are in qualitative agreement with experimental observations.

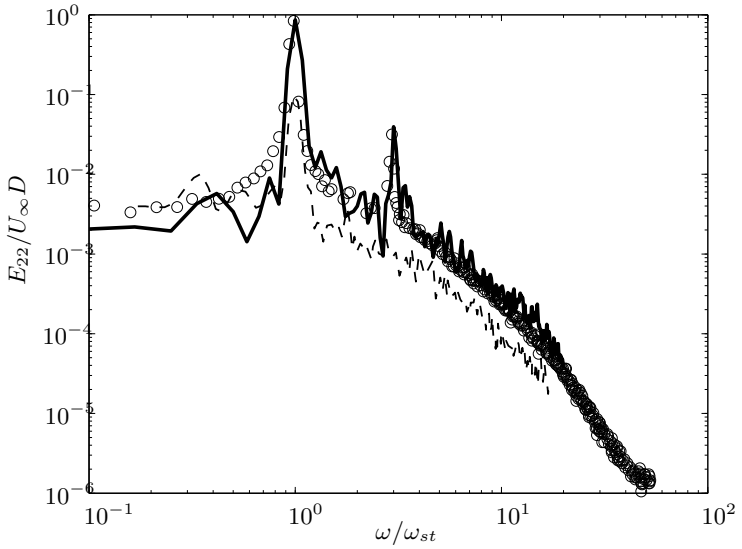

FIGURE 1. Energy spectra of vertical velocity as a function of non-dimensional frequency. ——— , Present LES ($M = 0.2$); - - - - , LES of Kravchenko & Moin (1998); ∘ , Experiment (Ong & Wallace 1999).

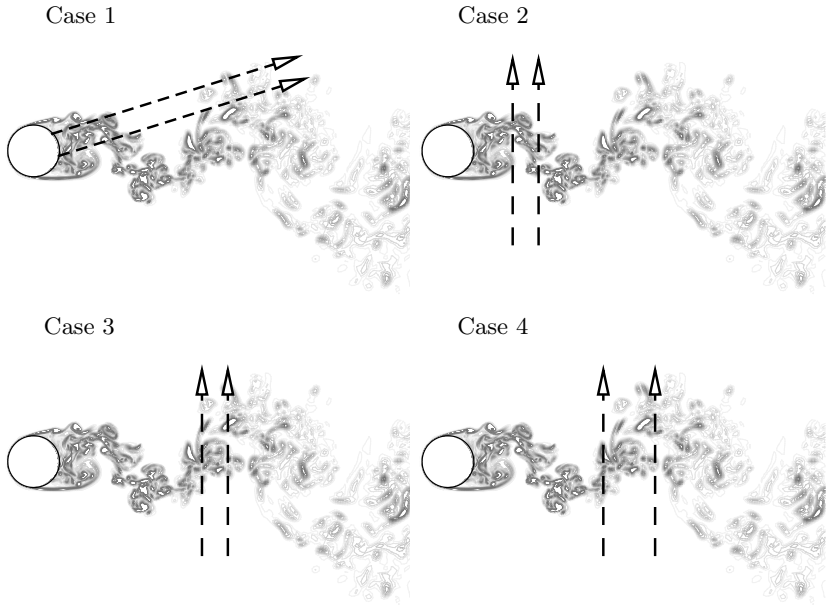

FIGURE 2. Schematics of optical propagation for four different cases. Arrows represent directions of optical propagation. The distance between the two arrows corresponds to the diameter of the optical aperture. The contours represent instantaneous vorticity magnitude in a spanwise plane.

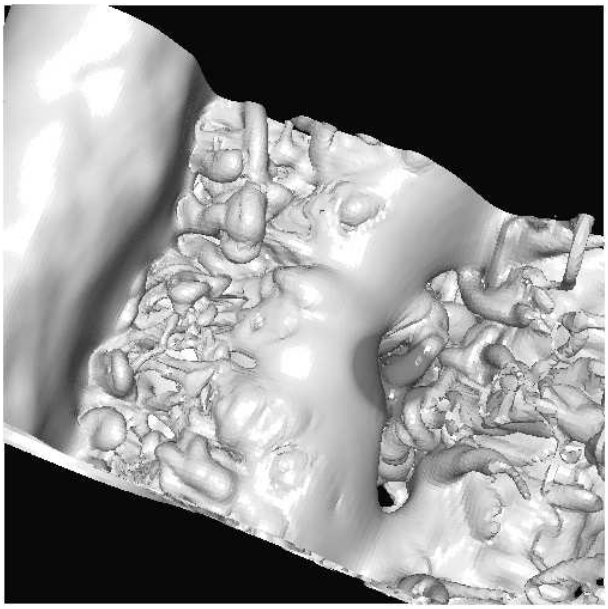

FIGURE 3. Instantaneous isosurfaces of density for $\rho = 0.98\rho_\infty$. The dark zone schematically represents the optical beam.

2.2. *Optical computation*

For optical analysis, four different cases are considered as shown schematically in Fig. 2. In the first case, an optical beam is emitted from the surface of the cylinder at an angle of approximately 17° with respect to the direction of downstream flow. For better numerical accuracy, the initial intensity of the beam is assumed to be a Gaussian profile that decays to $1/e^2$ times the maximum value at a distance of $0.15D$ from the optical axis. In our computations the optical intensity is truncated at $0.35D$ away from the axis where the intensity is less than 0.01% of the peak intensity. In the second case the optical beam of the same aperture diameter is shot vertically through the near wake behind the cylinder. The axis of the beam is $1.5D$ downstream from the cylinder axis. In the third case the beam is moved further downstream to $3.5D$ from the cylinder axis. Finally, in the fourth case the size of the optical aperture is doubled to $0.6D$ with its optical axis remaining in the same position as in Case 3. Figure 3 shows a snapshot of the fluctuating density field in the cylinder wake with an optical beam (corresponding to Case 3) marked as a dark spot.

A combination of ray tracing with Fourier optics, which has been used in previous computations (see, for example, Jones & Bender 2001), is an accurate tool to compute optical wave propagation in the parameter range of interest. In this method the domain of beam propagation is divided into two parts: the small near field in which ray tracing can be applied accurately, and the far field in which the density is assumed spatially uniform and Fourier optics can be applied. Spline interpolations are used to obtain the value of the density and its gradients along the ray path. Once ray tracing yields the distorted wavefront after passing the turbulence region, Fourier optics is used to find the far-field intensity pattern for given the optical wavelength and distance of propagation. The

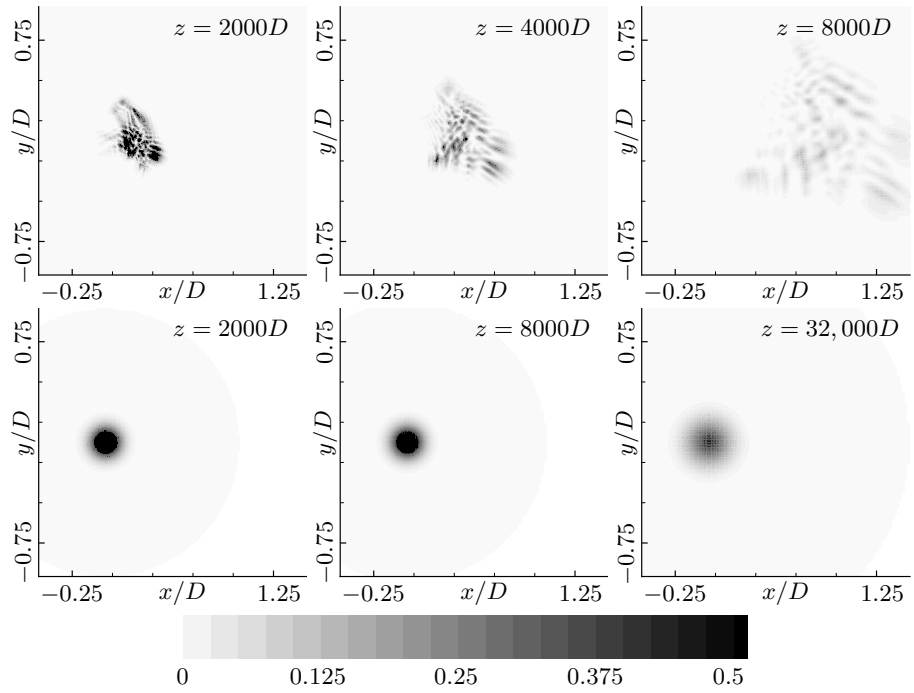

FIGURE 4. Instantaneous far-field intensity patterns for an aberrated beam corresponding to Case 1 (top) and a non-aberrated beam (bottom) at different distances of propagation. The optical wavelength is $2.5 \times 10^{-6} D$. The intensity levels are normalized by the peak intensity at the aperture where a Gaussian profile is assumed.

Fraunhofer approximation (see Saleh & Teich 1991) is used if the distance of propagation is sufficiently large; otherwise our Fourier optics is based on the exact solution of wave equation.

In the optical calculation the near field is taken to be within $20D$, while the far-field distance varies from $10^3 D$ to infinity. The optical wavelengths considered vary from $2.5 \times 10^{-6} D$ to $4 \times 10^{-5} D$. We assume a linear relation between the index of refraction and density (see Wolf & Zizzis 1978) in the non-dimensional form: $n - 1 = 2.8 \times 10^{-4} \times \rho/\rho_\infty$, where ρ and ρ_∞ are the instantaneous and freestream densities, respectively. In general, the constant in the relation depends on the reference density ρ_∞, which is based on air under atmospheric conditions in this study. Depending on the optical wavelength, 256 to 2048 Fourier modes in each direction in the plane perpendicular to the beam are used for far-field computations.

2.2.1. *Instantaneous results*

Figure 4 shows the spatial evolution of the far-field intensity of a distorted beam in Case 1 and contrasts it with that of an undistorted one, for an optical wavelength of $2.5 \times 10^{-6} D$. The distorted beam shows a highly irregular and speckled intensity pattern, as described by Zeldovich *et al.* (1995). After a sufficient distance of transmission, the distortion leads to a significant loss of intensity. The beam starts to diverge at $4000D$. In contrast, the undistorted beam remains focused for a distance of up to approximately $32,000D$. In other words, the effective range of the optical beam is reduced by one order

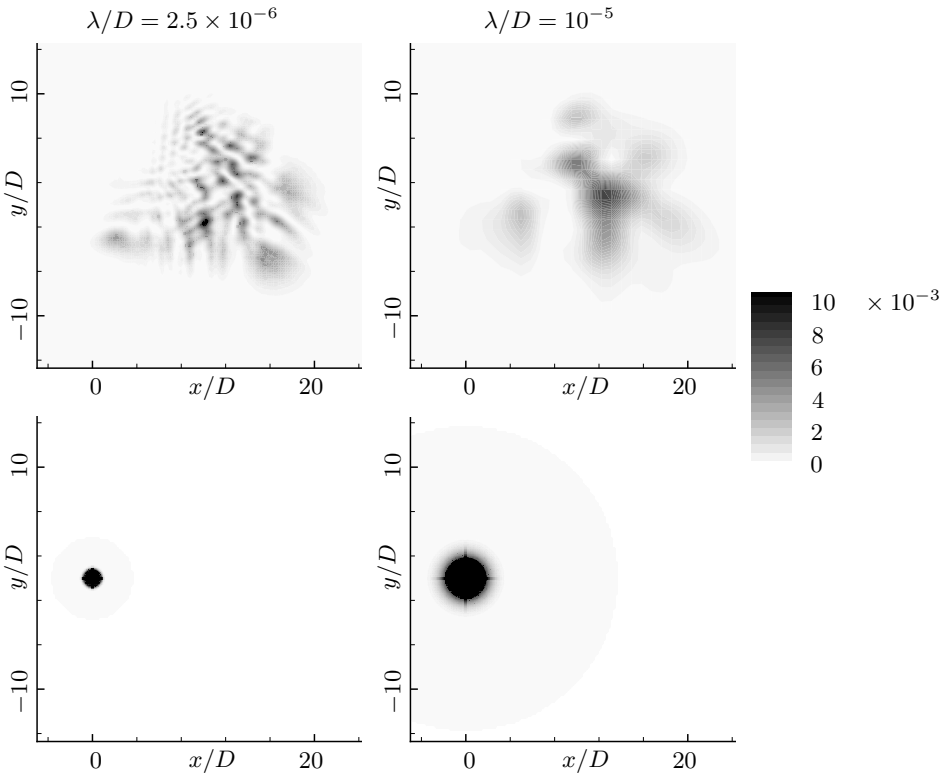

FIGURE 5. Instantaneous far-field intensity patterns for Case 1 for two different optical wavelengths (top) in comparison to undistorted beam patterns (bottom). The propagation distance of the beam is $10^5 D$, where the Fraunhofer approximation holds. The intensity levels are normalized by the peak intensity at the aperture.

of magnitude due to turbulence-induced distortions. Figure 5 shows the far-field intensity patterns for the same beam configuration with two different optical wavelengths. For the shorter wavelength beam (left) the interference patterns show smaller-scale oscillations, while the global structure of the patterns is nearly the same for both wavelengths. The speckled pattern appears at optical wavelengths smaller than $10^{-5}D$ and as expected, from diffraction theory, the speckle size was found to be approximately proportional to the wavelength.

Figure 6 shows the effect of optical aperture diameter on the instantaneous intensity pattern by comparing distortions in cases 3 and 4 induced by the same instantaneous flowfield. By changing the aperture, while the qualitative spread of the beam is not changed, the speckle sizes and the interference pattern are changed significantly.

The above results illustrate that aero-optical distortions are strongly dependent on parameters such as the optical wavelength, distance of propagation, and aperture diameter. In a related study, Mani *et al.* (2006) derived several analytical relations between the spread of a distorted beam and these parameters, as well as the statistics of the flow. For statistical study of optical distortions, those relations can help reduce the computational effort by providing algebraic descriptions. However, in this study, we present more gen-

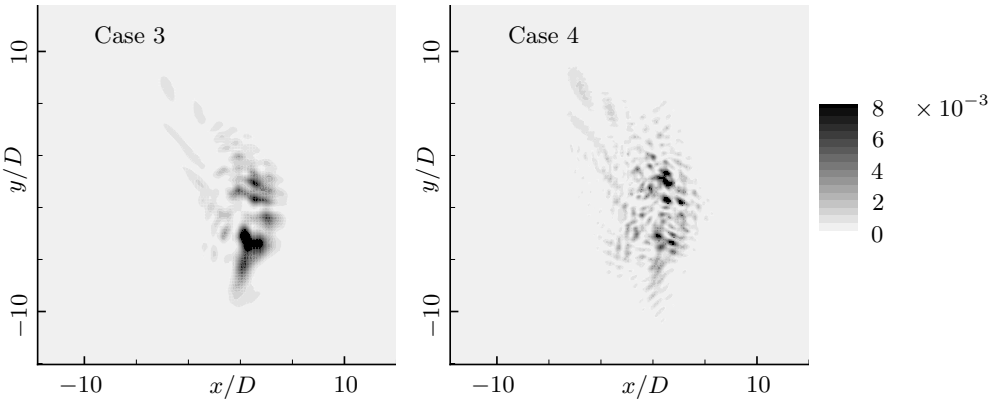

FIGURE 6. Comparison of instantaneous far-field intensity patterns for cases 3 and 4 where the only difference is the diameter of the optical aperture. The propagation distance of the beams is $10^5 D$ and the optical wavelength is $2.5 \times 10^{-6} D$.

eral statistics of optical distortions by examining the time averaged intensity pattern. We limit ourselves to the case of the Fraunhofer limit for distance of propagation in order to reduce the parameter space by one dimension. A detailed description, including different distances of propagation and the effect of distortion on the range of optical beams, is given in Mani *et al.* (2006).

2.2.2. *Time averaged statistics*

Figure 7 shows time averaged intensities for three wavelengths in the far field for Case 1 and compares them against the intensities of undistorted beams. As expected, for all the wavelengths studied, the undistorted beams provide higher intensities in the far field. It can be seen that for the case of undistorted beams, diffraction causes the longer wavelength beams to spread more. As a result, when there is no distortion, for shorter wavelength beams we have higher intensity, which translates to better performance of the optical device. In contrast, for the case of distorted beams the effect of the optical wavelength on the peak intensity is not as strong and is not monotone with the wavelength. In fact, there is an optimal wavelength that leads to a maximum time averaged peak intensity.

Figure 8 compares the time averaged intensity for the four different cases. The plots also provide the statistics of the tilt corrected patterns, where the tilt error is removed at every time step. From the plots it can be concluded that the tilting effect is significant, but not necessarily dominant, compared to the spreading effect. In general as the beam is moved further downstream, the aero-optical distortions decrease due to the decay of the turbulence. A comparison of cases 3 and 4 shows that the time averaged intensity pattern without tilt removal is almost unchanged, eventhough the aperture size is changed. This is in contrast to the case of undistorted beams for which larger aperture size leads to better focus properties. This is most likely due to the fact that the aero-optical effect dominates the diffraction effect in this regime. Furthermore, the improvement of the beam quality by tilt removal is less prominent in Case 4 compared to Case 3. Since tilt removal acts as a high-pass filter with filter size of the order of aperture diameter, this observation suggests that the optically important structures at this particular location

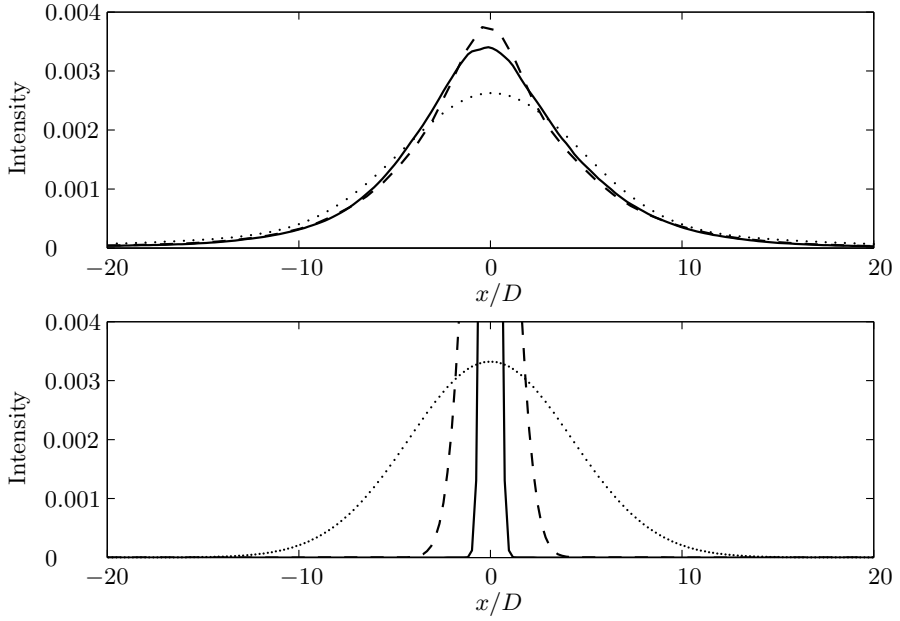

FIGURE 7. Time averaged and tilt removed intensities for different optical wavelengths (top) in comparison with those of undistorted beams (bottom). To obtain a 1-D plot, the 2-D intensity patterns are integrated in the y direction shown in Fig. 4, which is the homogeneous direction of the flow. The plots correspond to Case 1 at a distance of $10^5 D$. ——— , $\lambda/D = 2.5 \times 10^{-6}$; – – – – , $\lambda/D = 10^{-5}$; ····· , $\lambda/D = 4 \times 10^{-5}$.

are dominated by length scales smaller than or comparable to the aperture size in Case 3 (for more information, see Siegenthaler *et al.* 2005).

2.3. *Grid convergence*

A grid convergence study was conducted to ensure that the unresolved scales in the LES are optically unimportant. The resolution was doubled in every direction to a grid of $575 \times 400 \times 96$ in the wall normal, azimuthal, and spanwise directions, respectively. Since aero-optical distortions are due to density fluctuations, we compare density spectrum from the coarse mesh simulation with that from the fine mesh simulation. It can be seen that increasing grid resolution improves the capturing of small-scale fluctuations of density. However, the aero-optical effect of the additional small-scale fluctuations appears to be negligible compared to the effect of larger scales, as shown in Fig. 10, which compares the time averaged intensities from the two simulations. This indicates that the coarser mesh simulation has satisfactory resolution in terms of capturing the important aero-optical effects.

3. Conclusion

In summary, a high-resolution LES of compressible flow past a circular cylinder at $Re_D = 3900$ and $M = 0.4$ has been performed, and the flow statistics have been validated

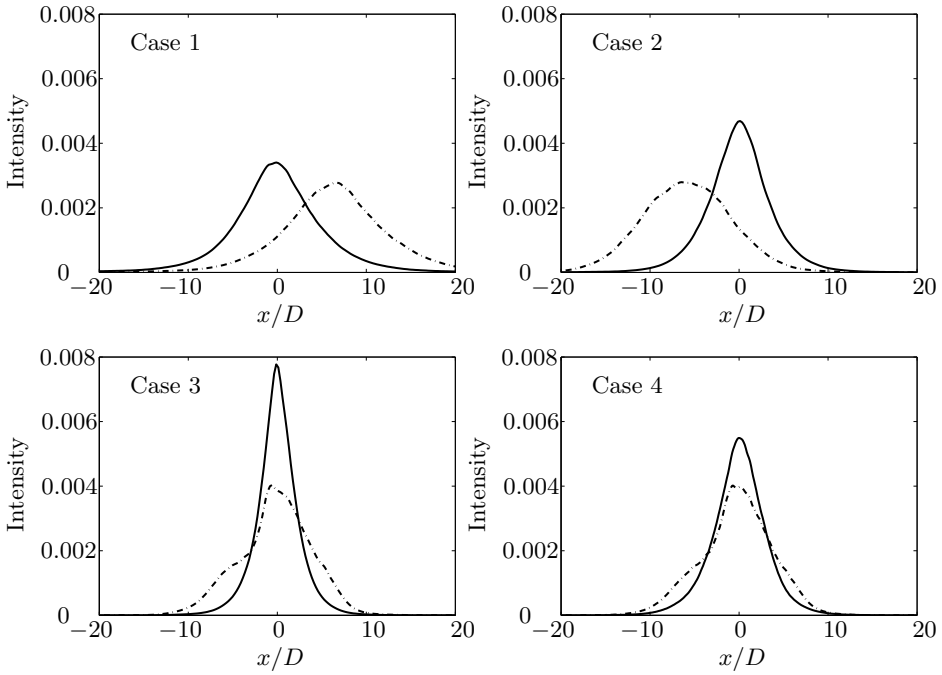

FIGURE 8. Time averaged intensity for optical wavelength of $2.5 \times 10^{-6}D$ for the four cases shown in Fig. 2. The 2-D intensity patterns are integrated in one direction (see Fig. 7 caption). ——— , tilt removed; —·— , original.

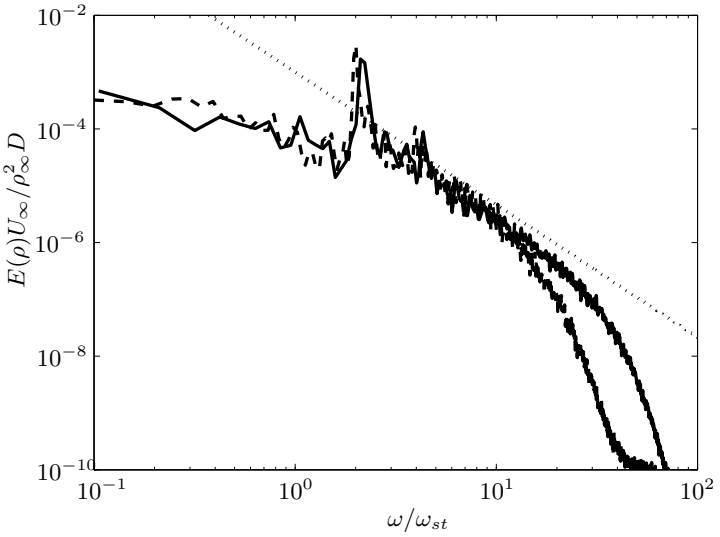

FIGURE 9. Density spectra at $5D$ downstream of the cylinder for the coarse and fine mesh simulations. - - - - , Coarse mesh simulation; ——— , Fine mesh simulation; ····· , $-7/3$ law.

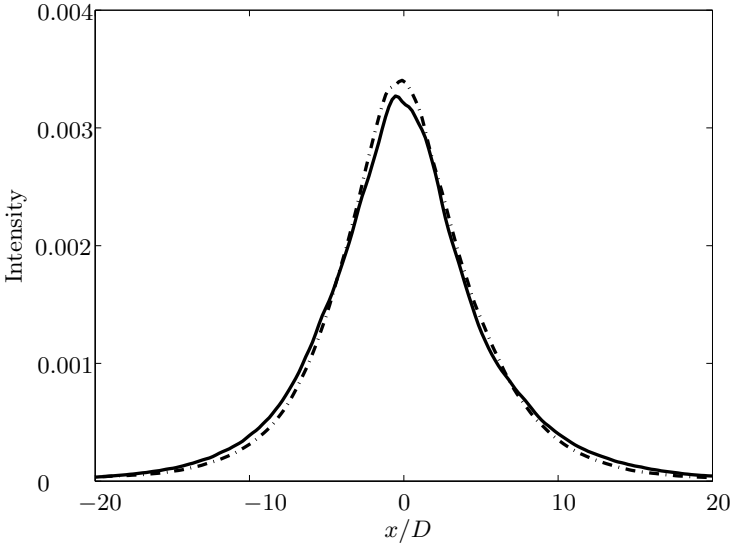

FIGURE 10. Comparison of time averaged far field intensities for $\lambda/D = 2.5 \times 10^{-6}$ and propagation distance of $10^5 D$ for the coarse mesh (—·—) and fine mesh (———) simulations.

against previous experimental and numerical results. Using the space-time history of the refractive index (density) field from LES, instantaneous and statistical descriptions of the flow-induced optical aberrations have been studied for different optical wavelengths and propagation distances.

Our results show that the turbulent wake flow can significantly degrade the performance of optical beams. Depending on the wavelength, the maximum irradiance of the optical beam can be reduced by one or two orders of magnitude. Also, turbulence can severely limit the effective range of an optical beam. Unlike the undistorted case where shorter wavelengths are desirable for greater depth of focus, for an aberrated beam there is an optimal wavelength for the highest peak intensity.

Acknowledgment

This work was supported by the Air Force Office of Scientific Research under grant Nos. F49-620-03-1-0132 and FA9550-06-1-0147. Computer time was provided by NAS at NASA Ames Research Center.

REFERENCES

BEAUDAN, P. & MOIN, P. 1994 Numerical experiments on the flow past a circular cylinder at sub-critical Reynolds number. *Tech. Rep.* TF-62. Department of Mechanical Engineering, Stanford University, Stanford, California.

CATRAKIS, H. J. & AGUIRRE, R. C. 2004 New interfacial fluid thickness approach in aero-optics with applications to compressible turbulence. *AIAA J.* **42**, 1973–1981.

CHERNOV, L. A. 1960 *Wave Propagation in a Random Medium*. New York, NY: McGraw-Hill.

Cheung, K. & Jumper, E. J. 2004 High temporal bandwidth optical wavefront sensor technologies. Proceedings of 2004 AFOSR Contractors' Meeting in Turbulence and Rotating Flows, Denver, Colorado, Aug. 4–5, 2004.

Childs, R. E. 1993 Prediction and control of turbulent aero-optical distortion using large eddy simulation. AIAA Paper 93-2670.

Dimotakis, P. E., Catrakis, H. J. & Fourguette, D. C. 2001 Flow structure and optical beam propagation in high-Reynolds number gas-phase shear layer and jets. *J.Fluid Mech.* **433**, 105–134.

Fitzgerald, E. J. & Jumper, E. J. 2004 The optical distortion mechanism in a nearly incompressible free shear layer. *J. Fluid Mech.* **512**, 153–189.

Gilbert, K. G. 1982 Overview of aero-optics. In *Progress in Astronautics and Aeronautics: Aero-Optical Phenomena*, Vol. 80, 1–9.

Gordeyev, S., Jumper, E. J., Ng, T. T. & Cain, A. B. 2003 Aero-optical characteristics of compressible, subsonic turbulent boundary layers. AIAA Paper 2003-3606.

Gordeyev, S., Jumper, E. J., Ng, T. T. & Cain, A. B. 2004 Optical disturbances caused by transonic separated boundary layer behind a 20-degree ramp: physics and control. AIAA Paper 2004-0472.

Jones, M. I. & Bender, E. E. 2001 CFD-based computer simulation of optical turbulence through aircraft flowfields and wakes. AIAA Paper 2001-2798.

Jumper, E. J. & Fitzgerald, E. J. 2001 Recent advances in aero-optics. *Progress in Aerospace Sciences* **37**, 299–339.

Kravchenko, A. G. & Moin, P. 1998 B-spline methods and zonal grids for numerical simulations of turbulent flows. *Tech. Rep.* TF-73. Department of Mechanical Engineering, Stanford University, Stanford, California.

Lilly, D. K. 1992 A proposed modification of the Germano subgrid-scale closure method. *Phys. Fluids A* **4**, 633–635.

Mani, A., Wang, M. & Moin, P. 2006 Statistical description of free-space propagation for highly aberrated optical beams. *J. Opt. Soc. Am. A* **23**, 3027–3035.

Mittal, R. & Moin, P. 1997 Suitability of upwind-biased finite-difference schemes for large-eddy simulation of turbulent flows. *AIAA J.* **35**, 1415–1417.

Moin, P., Squires, K., Cabot, W. & Lee, S. 1991 A dynamic subgrid-scale model for compressible turbulence and scalar transport. *Phys. Fluids A* **3**, 2746–2757.

Nagarajan, S., Lele, S. K. & Ferziger, J. H. 2003 A robust high-order compact method for large eddy simulation. *J. Comput. Phys.* **191**, 392–419.

Ong, L. & Wallace, J. 1999 The velocity field of the turbulent very near wake of a circular cylinder. *Experiments in Fluids* **20**, 441–453.

Rizzetta, D. P., Visbal, M. R. & Blaisdell, G. A. 2003 A time-implicit high-order compact differencing and filtering scheme for large-eddy simulation. *Int. J. Numer. Methods Fluids* **42**, 665–693.

Saleh, B. E. A. & Teich, M. C. 1991 *Fundamentals of Photonics*, 121–122. John Wiley & Sons, Inc.

Siegenthaler, J., Gordeyev, S. & Jumper, E. 2005 Shear layers and aperture effects for aero-optics. AIAA Paper 2005-4772.

Sinha, N., Arunajatesan, S., Seiner, J. M. & Ukeiley, L. S. 2004 Large-eddy simulations of aero-optic flow fields and control application. AIAA Paper 2004-2448.

Smith, R. & Truman, C. 1990 Prediction of optical phase degradation using a turbulent

transport equation for the variance of index-of-refraction fluctuations. AIAA Paper 90-0250.

Sutton, G. W. 1969 Effect of turbulence fluctuations in an optically active fluid medium. *AIAA J.* **7**, 1737–1743.

Tatarski, V. I. 1961 *Wave Propagation in a Turbulent Medium*. New York, NY: McGraw-Hill.

Tromeur, E., Garnier, E., Sagaut, P. & Basdevant, C. 2003 Large eddy simulations of aero-optical effects in a turbulent boundary layer. *Journal of Turbulence* **4** (005).

Truman, C. R. 1992 The influence of turbulent structure on optical phase distortion through turbulent shear flows. AIAA Paper 92-2817.

Truman, C. R. & Lee, M. J. 1990 Effects of organized turbulence structures on the phase distortion in a coherent optical beam propagating through a turbulent shear flow. *Phys. fluids A* **2**, 851–857.

Wolf, W. & Zizzis, G. J. 1978 *The Infrared Handbook*, pp. 16–24.

Zeldovich, B. Y., Mamaev, A. V. & Shkunov, V. V. 1995 *Speckle-wave Ineractions in Application to Holography and Nonlinear Optics*. Boca Raton, FL: CRC Press.